Numerical irreversibility in self-gravitating small N-body systems, II: Influence of instability affected by softening parameters

Numerical irreversibility in self-gravitating small N-body systems. (II). Influence of instability affected by softening parameters.

Nobuyoshi Komatsu [a], Takahiro Kiwata [a] and Shigeo Kimura [b]

[a] *Department of Mechanical Systems Engineering, Kanazawa University, Kakuma-machi, Kanazawa, Ishikawa 920-1192, Japan*

[b] *The Institute of Nature and Environmental Technology, Kanazawa University, Kakuma-machi, Kanazawa, Ishikawa 920-1192, Japan*

Abstract

We investigate the fundamental characteristics of numerical irreversibility appearing in self-gravitating small N-body systems by means of a molecular dynamics method from the viewpoint of time-reversible dynamics. We reconsider a closed spherical system consisting of 250 point-particles interacting through the Plummer softened potential. To investigate the characteristics of numerical irreversibility, we examine the influence of the instability affected by the softening parameter for the softened potential (the instability considered here is the instability of a dynamical system in chaos theory, e.g., a separation rate of the distance between two nearby trajectories in phase space or speed space). To this end, under the restriction of constant initial energy, the softening parameter for the Plummer softened potential is varied from $0.005R$ to $0.050R$, where R is the radius of the spherical container. We first confirm that the size of the softening parameter, i.e., the deviation of the potential from a pure gravitational potential, influences the virial ratio, the density, the pressure on the spherical container, etc., during an early stage of the relaxation process. Through a time-reversible simulation based on a velocity inversion technique, we demonstrate that numerical irreversibility due to round-off errors appears more rapidly with decreasing softening parameter. This means that the higher the instability of the system or the higher the separation rate of the distance between two nearby trajectories, the earlier the memory of the initial conditions is lost. We show that the memory loss time t_{m}, when the simulated trajectory completely forgets its initial conditions, increases approximately linearly with the timescale of the chaotic system, i.e., the Lyapunov time t_{λ}. In a small self-gravitating system, propagation of numerical irreversibility or loss of reversibility depends on both the energy state of the system and the instability affected by the softening parameter.

Key words: Self-gravitating system, Irreversibility, Instability, Round-off errors,

PACS: 04.40.-b, 05.70.Ln, 05.40.Ca, 02.70.Ns, 05.45.Pq

1 Introduction

Stellar self-gravitating N-body systems have attracted considerable research attention due to the fact that they exhibit properties quite different from short-range interacting systems, e.g., negative specific heat, violent relaxation and non-equilibrium nonextensive statistical mechanics [1–7]. Since N-body problems cannot be solved analytically, numerical simulations are important for studying N-body systems [8,9]. For example, in 1963, Aarseth simulated dynamical evolution of clusters of galaxies using the Plummer softened potential $\sim -1/(r^2 + r_0^2)^{1/2}$, where r_0 and r represent the softening parameter and the distance between particles, respectively [10]. However, it is known that numerical simulations inherently include round-off errors and that numerical irreversibility arises from the round-off errors, even in time-reversible systems.

In the 1960s, Miller [11,12] examined irreversibility in small stellar dynamical systems and showed that numerical errors grow exponentially with time. Subsequently, many researchers, e.g., Lecar [13], Standish [14], Gurzadyan et al. [15], Kandrup [16], have investigated self-gravitating systems from the viewpoint of instability [17–29]. The instability discussed by them is the instability of a dynamical system in chaos theory, e.g., a separation rate of the distance between two nearby trajectories in phase space. However, irreversibility appearing in self-gravitating N-body systems has not yet been clarified from the viewpoint of time-reversible dynamics. In fact, even in short-range interacting systems [30–32], the influence of round-off errors or numerical irreversibility has not been investigated quantitatively, except for a few simple models [33–35] or for the works by the present authors [36–38].

Accordingly, to bridge the gap between short-range and long-range interacting systems, we investigated the numerical irreversibility appearing in self-gravitating N-body systems through a time-reversible simulation [39]. In a previous paper (Physica A 387 (2008) 2267; hereafter Paper I), we examined the influence of energy states and the integration step size Δt. In particular, in Paper I, to investigate the fundamental characteristics of numerical irreversibility, the softening parameter r_0 for the Plummer softened potential was fixed, since r_0 affects the instability of the system. That is, we have not examined the influence of the instability affected by the softening parameter on

Email address: komatsu@t.kanazawa-u.ac.jp (Nobuyoshi Komatsu).

the numerical irreversibility. However, we can expect that the instability of a system, as suggested by Krylov [40], is closely related to irreversibility or loss of reversibility [31].

In most self-gravitating N-body simulations, in order to avoid noisy force estimates due to close encounters between particles or to simulate collisionless systems, the true potential $\sim -1/r$ is replaced by an artificially softened potential, e.g., $\sim -1/(r^2 + r_0^2)^{1/2}$. The influence of such softening parameters on N-body simulations has been investigated by Standish [14], Suto [19] and many other researchers [41–46]. In particular, the influence of the softening parameter on instability was examined in detail by Kandrup et al. [21] and Goodman et al. [22]. Recently, optimal softening for N-body simulations has been examined and discussed in an effort to minimize average errors in force calculations [47–51]. However, numerical irreversibility or loss of reversibility has not been investigated from the viewpoint of time-reversible dynamics. Moreover, although the instability affected by the softening parameter has been generally studied using phase trajectories, a relationship between the instability and numerical irreversibility has not been clear and not been investigated quantitatively. This is because the instability of the system isn't irreversibility itself, even if they could be closely related to each other. Therefore, we can expect that it is worthwhile to study numerical irreversibility and to examine the relationship between them quantitatively.

In this context, to clarify the relationship between irreversibility and instability affected by the softening parameter, we investigate numerical irreversibility appearing in a self-gravitating system through a time-reversible simulation. We consider a system consisting of N point-particles enclosed in a spherical container of radius R with reflecting walls [52–57]. To simulate an unstable system, the softening parameter r_0 is varied between $0.005R$ and $0.050R$, under a restriction of constant initial energy. That is, we examine the influence of the instability affected by the softening parameter on numerical irreversibility for a deeper understanding of simulations of self-gravitating N-body systems; i.e., through the simulation, we investigate numerical irreversibility appearing in those unstable systems.

The present paper is organized as follows. In Section 2, we give a brief review of numerical techniques for simulating a self-gravitating system enclosed in a spherical container with a reflecting wall. We describe the initial conditions for the simulation and a velocity inversion technique for time-reversible simulations. We also define several parameters for observing the unstable and irreversible behavior of a system. In Section 3, the simulation results are presented. Through a typical relaxation process, we first examine the influence of the softening parameter in Section 3.1. In Section 3.2, based on the time-reversible simulation, the relationship between the numerical irreversibility and instability of the system is investigated and discussed. In Section 3.3, the

influence of the time step or the integration step size Δt is examined. Finally, we present our conclusions.

2 Methods

We consider a system consisting of N point-particles enclosed in a spherical container of radius R with reflecting (adiabatic) walls, i.e., the Antonov problem [1]. Although a method to simulate the Antonov problem has been described in Paper I, the details in the present simulation are slightly different. Therefore, in this section, we briefly review the present method.

2.1 Numerical models

To simulate a self-gravitating system, we integrate the set of classical equations of motion for the particles interacting through the Plummer softened potential. The Plummer softened potential Φ is given by

$$\Phi = -\frac{1}{\sqrt{r^2 + r_0^2}}, \tag{1}$$

where r and r_0 represent the distance between particles and the softening parameter, respectively. It is well-known that variations in the softening parameter r_0 influence the instability of a self-gravitating system [19–24]. Accordingly, in order to examine several systems, r_0 is varied from $0.005R$ to $0.050R$. In particular, r_0 is set to be $0.005R$, $0.010R$, $0.020R$ and $0.050R$, respectively.

In the present system, the total energy E is defined as

$$E = E_{\rm KE} + E_{\rm PE} = \sum_i^N \frac{m_i v_i^2}{2} - \sum_{i<j}^N \frac{G m_i m_j}{\sqrt{r_{ij}^2 + r_0^2}}, \tag{2}$$

where $E_{\rm KE}$, $E_{\rm PE}$ and m_i represent kinetic energy, potential energy and the mass of the i-th point-particle, respectively. G, v_i and r_{ij} represent the gravitational constant, the speed of the i-th particle and the distance between the i-th and j-th particles, respectively. In this study, we set the mass of each particle to m. So that we can apply traditional conventions for self-gravitating systems, we define the total rescaled energy ε as

$$\varepsilon = \varepsilon_{\rm KE} + \varepsilon_{\rm PE} = E\frac{R}{GM^2} = E\frac{R}{G(mN)^2}, \tag{3}$$

where M, $\varepsilon_{\rm KE}$ and $\varepsilon_{\rm PE}$ represent the total mass mN, rescaled kinetic and potential energies, respectively. In our simulations, the unit of time is chosen

so that the gravitational constant is unity; i.e., $G \times [\mathrm{M}][\mathrm{L}]^{-3}[\mathrm{T}]^2 = 1$, where [M], [L] and [T] represent the units of mass, length and time, respectively. Therefore, the unit of time is $\sqrt{R^3/(Gm)}$, since the units of mass and length are m and R in the present paper [58]. To ensure generality of the system, we set the units such that $G = R = m = 1$ [54].

The set of equations of motion is integrated using Verlet's algorithm (i.e., the leapfrog algorithm), since the scheme of this algorithm is time-reversible. Through the simulations, the interparticle forces are calculated directly at each time step, to avoid irreversibility due to the simulation procedure. In the spherical container, to mimic a reflecting wall, the radial component of the velocity of a particle is reversed when it reaches the reflecting wall [57]. In our simulations, when the position of the particle is located outside of the spherical container, the position is reversed to mimic the reflecting wall (the detail is summarized in Appendix A). Accordingly, we can avoid irreversibility appearing in the simulations apart from that due to round-off errors.

In this study, we consider a small system consisting of $N = 250$ point-particles in a spherical container of radius $R = 1$. In particular, to observe the averaged behavior of the system, all the results are averaged over 100 simulations with identically prepared initial setups [59]. In the present system, the crossing time τ_c and the relaxation time τ_r are evaluated as $\tau_c \approx 1/\sqrt{G\rho} = 1/\sqrt{\rho}$ and $\tau_r \approx (0.1N/\ln N)\tau_c$, respectively, where ρ represents the density of the system [3]. In our units, the crossing and relaxation times are $\tau_c \approx 0.1$ and $\tau_r \approx 0.6$, respectively. It should be noted that this approximation for the relaxation time depends on an assumption that the system is in an approximate virial equilibrium state.

For simulating a self-gravitating system, a double precision floating point real number is used. In order to keep the total energy variation within 0.01% of its initial value, we set the time step or the integration step size Δt to 10^{-5}. However, in Section 3.3, to examine an influence of the integration step size, Δt is varied from 10^{-4} to 10^{-6}, for $r_0 = 0.005R$.

Note that we employ the fixed-time-step integrator, i.e., Verlet's algorithm, in order to study the present self-gravitating system from the viewpoint of time-reversible dynamics. In the system, the initial velocity distribution approaches approximately the Maxwell-Boltzmann one, during an early stage of the relaxation process (i.e., several relaxation times). However, during this stage, several particles affected by strong collisions (i.e., close encounters) can influence trajectories of the particles significantly, even if we observe an averaged behavior of the system. That is, we could expect that the integration step size by the fixed-time-step integrator influences the trajectory, since a smaller integration step size can simulate such a rapid change of the trajectory. Therefore, we investigate the influence of the integration step size for

the present system, although we have examined the influence for the similar system in Paper I.

2.2 Initial setup and parameters for simulations

To simulate time evolution of a system, the system is initially set to be in a highly non-equilibrium state with all the particles initially distributed randomly in the spherical container, based on a spherically symmetric uniform density profile. Moreover, the initial velocity distribution is assumed to be that of a non-equilibrium state. That is, for an initial setup, all the particles are set to have a velocity of $|\mathbf{v}_0|$ but with a random direction. The initial velocities $\mathbf{v}_0$ are set to keep the initial virial ratio as

$$\frac{2E_{\mathrm{KE}_0}}{|E_{\mathrm{PE}_0}|} = \frac{2\varepsilon_{\mathrm{KE}_0}}{|\varepsilon_{\mathrm{PE}_0}|} = 0.5. \tag{4}$$

Thereafter, to keep the total momentum and the total angular momentum 0, the velocities of the particles are slightly modified, taking into account the spherically symmetric uniform density profile. The details for the initial setup are summarized in Table 1. The total rescaled energy ε is fixed at $\varepsilon \approx -0.47$, and could be lower than the collapse energy ε_{coll} [60].

It should be noted that, in this paper, we consider the system consisting of N point-particles enclosed in a spherical container with the reflecting wall. Accordingly, the virial theorem for the present system is given as

$$2E_{\mathrm{KE}} + E_{\mathrm{PE}} = 4\pi R^3 P_{\mathrm{wall}}, \tag{5}$$

where P_{wall} represents the pressure on the reflecting wall [54,56]. That is, unlike a system without the wall, $2E_{\mathrm{KE}} + E_{\mathrm{PE}}$ isn't 0, because of the reflecting wall. The pressure on the reflecting wall at time t can be evaluated as

$$P_{\mathrm{wall}}(t) = \frac{\sum_{\hat{t}=t-t''/2}^{\hat{t}=t+t''/2} 2mv_{\mathrm{r}}(\hat{t})}{4\pi R^2 t''} = \frac{\sum_{\hat{t}=t-t''/2}^{\hat{t}=t+t''/2} mv_{\mathrm{r}}(\hat{t})}{2\pi R^2 t''}, \tag{6}$$

Table 1
Technical details for the initial setup.

r_0/R	ε	$\varepsilon_{\mathrm{KE}_0}$	$\varepsilon_{\mathrm{PE}_0}$
0.005	-0.4718 ± 0.0097	0.1573 ± 0.0007	-0.6291 ± 0.0098
0.010	-0.4715 ± 0.0096	0.1571 ± 0.0007	-0.6286 ± 0.0096
0.020	-0.4705 ± 0.0094	0.1568 ± 0.0007	-0.6274 ± 0.0094
0.050	-0.4662 ± 0.0087	0.1554 ± 0.0007	-0.6216 ± 0.0087

The errors indicate the 68% confidence level in terms of the normal error distribution from 100 simulations.

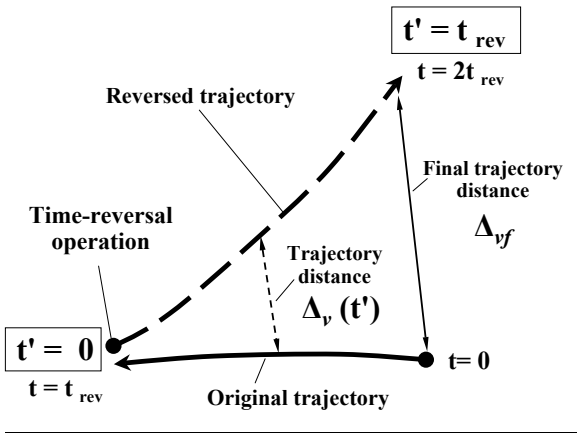

Fig. 1. Sketch of the trajectory distance in speed space.

where $v_{\rm r}(\hat{t})$ is the summation of the radial components of the velocities of all particles which are reflected by the wall, at each time step $\hat{t}$ [54]. In general, fluctuations in the instantaneous pressure are larger than those in other macroscopic parameters. Therefore, to reduce the large fluctuation in the pressure, the interval t'' in Eq. (6) is set to be $1000\Delta t$ steps.

To study numerical irreversibility due to round-off errors, we consider a typical problem including a time-reversal operation. For this purpose, the system is initially in a highly non-equilibrium state. During the time evolution of the system, the time-reversal operation is applied at a certain time, i.e., all the particles reverse their velocities instantaneously at a certain time $t_{\rm rev}$, and the system then evolves reversibly. If the system is reversible, the initial state should appear again at $2t_{\rm rev}$. However, if the system contains any irreversibility, such as numerical irreversibility, the initial state appears only incompletely or doesn't appear at all.

As in Paper I, we investigate the irreversible behavior through the time-reversible simulation by observing the distance between two nearby trajectories in speed space, namely, the original and reversed trajectories. As shown in Fig. 1, the original trajectory is taken as the trajectory before the time-reversal operation, i.e., from $t = 0$ to $t = t_{\rm rev}$. The reversed trajectory is taken as the trajectory after the time-reversal operation, i.e., from $t = t_{\rm rev}$ to $t = 2t_{\rm rev}$. The trajectory distance is given by

$$\Delta_v(t') = \frac{\sqrt{\frac{1}{N}\sum_{i=1}^{N}(v_i^{(\rm original)} - v_i^{(\rm reverse)})^2}}{< v(0) >}, \qquad (7)$$

where $v_i^{(\rm original)}$ and $v_i^{(\rm reverse)}$ are the speeds of the i-th particle at time t' for the original trajectory and for the reversed trajectory, respectively. The origin of t' is the time $t_{\rm rev}$ of the time-reversal operation. Note that $< v(0) >$ represents

the averaged speed at the time of the time-reversal operation, since the bracket $< X >$ represents the mean of X. From the trajectory distance at the final time $t' = t_{\rm rev}$, the final trajectory distance is given by

$$\Delta_{vf} = \Delta_v(t' = t_{\rm rev}). \tag{8}$$

For an overview of the loss of reversibility, we define a recovery rate R_R of the normalized ratio of velocity moments VM as

$$R_R \equiv \frac{\rm VM(2t_{rev}) - VM(t_{rev})}{\rm VM(0) - VM(t_{rev})}, \tag{9}$$

where

$$\rm VM(t) = \frac{vm(t) - vm_{MB}}{vm(0) - vm_{MB}}, \tag{10}$$

and

$$\rm vm(t) = \frac{< \mathbf{v}(t)^2 >^2}{< \mathbf{v}(t)^4 >}. \tag{11}$$

Note that vm(t) is the ratio of velocity moments at time t and $\rm vm_{MB}$ represents the specific value of the ratio of velocity moments corresponding to the Maxwell–Boltzmann velocity distribution. By using the recovery rate R_R, we can measure the loss of reversibility in the system. In other words, the smaller the recovery rate R_R, the more irreversible the system is.

In this paper, we observe an early stage of the relaxation process. That is, our simulation time $t \sim 1$ is sufficiently shorter than the time scale for a core-halo or a collapse state. For example, according to Ispolatov and Karttunen [55], a collapse time in the system with $N = 125 - 250$ particles and $r_0 = 0.005R$ is approximately $\sim 10^3$ relaxation times; i.e., in our units, the collapse time is approximately ~ 600.

3 Results

To study the influence of instability on numerical irreversibility, the softening parameter r_0 is varied from $0.005R$ to $0.050R$ (hereafter, from 0.005 to 0.050, since $R = 1$). In this section, the results are averaged over 100 simulations with identically prepared initial setups [59].

3.1 Early stage of the relaxation process

In order to investigate the influence of the softening parameter r_0, we observe the early stage of the relaxation process. For this purpose, we first examine

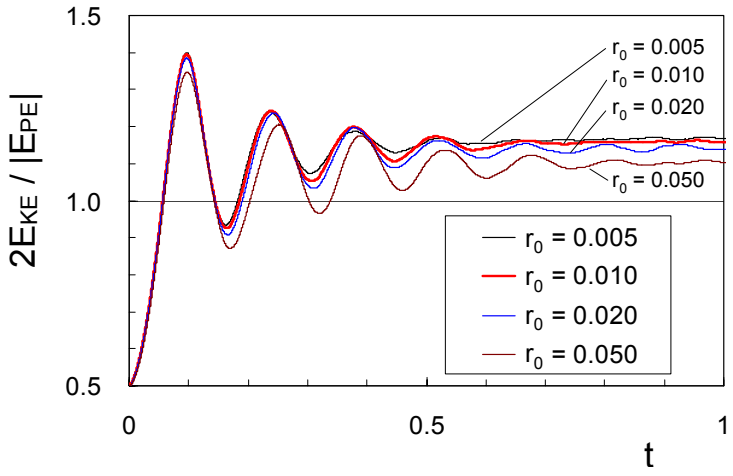

Fig. 2. (Color online) Time evolutions of the virial ratio $2E_{\rm KE}/|E_{\rm PE}|$, without the time-reversal operation.

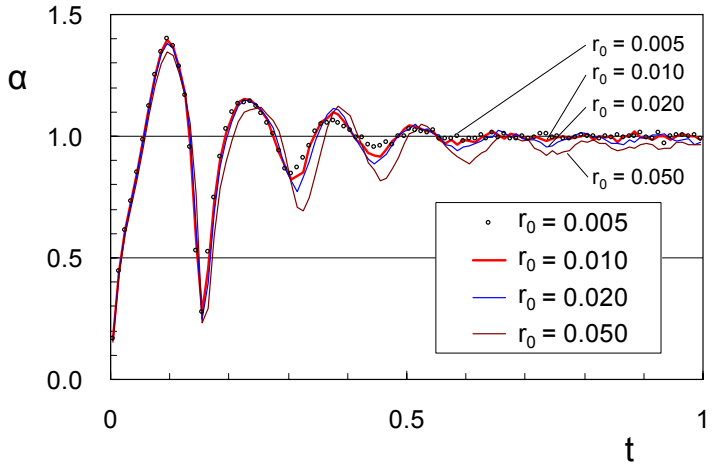

Fig. 3. (Color online) Time evolutions of the corrected virial ratio α $(=(2E_{\rm KE}-4\pi R^3 P_{\rm wall})/|E_{\rm PE}|)$, without the time-reversal operation. The values are plotted every $1000\Delta t$ steps, i.e., 0.01 (see the text).

the time evolution of the virial ratio $2E_{\rm KE}/|E_{\rm PE}|$, without the time-reversal operation. As shown in Fig. 2, each virial ratio increases quickly from the initial value 0.5 during the crossing time $\tau_c \approx 0.1$. Then, the value oscillates slightly and after $\tau_r \approx 0.6$ it gradually tends towards a certain quasi-steady state. Note that, since the relaxation time τ_r considered here depends on an assumption that the system is in an approximate virial equilibrium state, the present initial condition is different from this assumption. However, it seems that the behavior of the virial ratio is consistent with the two time scales of

the present self-gravitating system.

The values of $2E_{\rm KE}/|E_{\rm PE}|$ are larger than 1, at a quasi-steady state, e.g., at $t = 0.9 \sim 1.0$. We can expect that this deviation from 1 depends on the reflecting wall and the softening parameter, i.e., the deviation of the Plummer softened potential from the true potential, $\sim -1/r$. Therefore, to observe the influence of the softening parameter more clearly, we examine the corrected virial ratio, taking into account the pressure $P_{\rm wall}$ on the reflecting wall. For the present self-gravitating system, the corrected virial ratio α is given by

$$\alpha = (2E_{\rm KE} - 4\pi R^3 P_{\rm wall})/|E_{\rm PE}|. \tag{12}$$

At the virial equilibrium state with the true potential or with a pure gravitational potential, the value of α is 1. Figure 3 shows the time evolution of the corrected virial ratio α, without the time-reversal operation. In this figure, the values are plotted every $1000\Delta t$ steps, since the pressure is averaged not only over 100 simulations but also over $1000\Delta t$ steps, to reduce large fluctuations in the pressure. As shown in Fig. 3, the behaviors of α are similar to those of $2E_{\rm KE}/|E_{\rm PE}|$, although the values are different. As expected, at $t = 0.9 \sim 1.0$, the values of α approximately approach 1. That is, the present system is in an approximate virial equilibrium state at $t = 0.9 \sim 1.0$. However, it seems that, at $t = 0.9 \sim 1.0$, the deviation from 1 increases with increasing softening

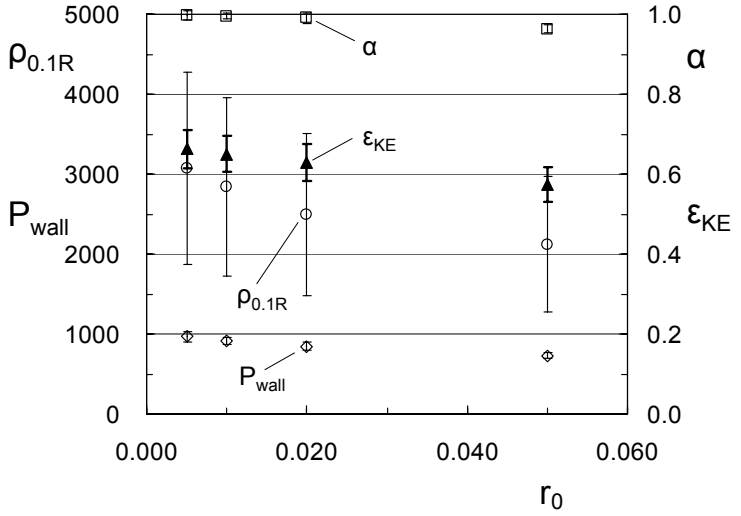

Fig. 4. Macroscopic parameters at the quasi-steady state. The open squares (□), diamonds (⋄) and circles(∘) represent the corrected virial ratio α, pressure $P_{\rm wall}$ on the reflecting wall and density $\rho_{0.1\rm R}$ in the inner region, respectively. The closed triangles (▲) represent the rescaled kinetic energy $\varepsilon_{\rm KE}$. The values are averaged over 100 simulations and over $t = 0.9$–1.0. As for α and $P_{\rm wall}$, the values are additionally averaged over $1000\Delta t$ steps. The error bars indicate the 68% confidence level in terms of the normal error distribution. The density $\rho_{0.1\rm R}$ represents an averaged density within a concentric sphere of radius $0.1R$.

parameter. This deviation depends on the size of the softening parameter, i.e., the deviation of the potential from $-1/r$.

To examine the influence of the softening parameter r_0 at the quasi-steady state, Fig. 4 shows the corrected virial ratio α, the pressure $P_{\rm wall}$ on the reflecting wall, the density $\rho_{0.1\rm R}$ in the inner region and the rescaled kinetic energy $\varepsilon_{\rm KE}$. As a result, we can confirm that the deviation of α from 1 increases with increasing softening parameter; i.e., α decreases with increasing r_0. Similarly, the pressure $P_{\rm wall}$, the density $\rho_{0.1\rm R}$ and the rescaled kinetic energy $\varepsilon_{\rm KE}$ decrease with increasing r_0. This is because strong collisions or close encounters could occur less frequently due to larger r_0. Accordingly, as shown in Fig. 2, $2E_{\rm KE}/|E_{\rm PE}| = 2\varepsilon_{\rm KE}/|\varepsilon - \varepsilon_{\rm KE}|$ decreases with r_0, because of the decrease in $\varepsilon_{\rm KE}$ at the quasi-steady state.

3.2 Instability and numerical irreversibility in time-reversible simulations

We now consider the time-reversible simulation of the present system. For this purpose, we examine time evolutions of the trajectory distance $\Delta_v(t')$ for $t_{\rm rev} = 1.0$; that is, the time-reversal operation is executed at $t = 1.0$ shown in Fig. 2. As a result, as shown in Fig. 5, all the curves increase exponentially with time t' at the early stage, where the origin of t' is the time $t_{\rm rev}$ of the time-reversal operation. In fact, in chaotic and unstable systems such as N-body systems, the trajectory distance grows exponentially with time as follows:

$$\Delta_v(t') = \Delta_v(0)e^{\lambda t'}, \tag{13}$$

where $\Delta_v(0)$ and λ represent the initial displacement and the maximum Lyapunov exponent in chaos theory [31,61], respectively. That is, at the early stage shown in Fig. 5, the slope of the trajectory distance corresponds to λ, i.e., the extent of the instability of the system. Therefore, as expected, the instability of the system increases with decreasing r_0. It should be noted that in this simulation $\Delta_v(0)$ arises from round-off errors. Based on λ, we can evaluate the Lyapunov time as

$$t_\lambda = 1/\lambda. \tag{14}$$

The Lyapunov time t_λ, which is calculated from Eq. (14), is summarized in Table 2. The table shows that t_λ increases monotonically with the softening parameter and, therefore, our result agrees well with previous studies [21,22]. We discuss the details below, including the memory loss time newly defined in this paper.

Through the time-reversible simulation, we examine numerical irreversibility appearing in the present self-gravitating system. To this end, Fig. 6 shows the relationship between the final trajectory distance $\Delta_{v\rm f}$ and time $t_{\rm rev}$ of the time-reversal operation, for various softening parameters. The figure shows that $\Delta_{v\rm f}$

Table 2
Lyapunov time t_λ for $t_{\rm rev} = 1.0$.

r_0	0.005	0.010	0.020	0.050
t_λ	0.005 ± 0.002	0.011 ± 0.002	0.022 ± 0.004	0.056 ± 0.006

To calculate the Lyapunov time t_λ, the maximum Lyapunov exponent λ was computed from an exponential part of each curve shown in Fig. 5. For $r_0 = 0.005$, 0.010, 0.020 and 0.050, we employed the exponential parts of $t' = 0.05$–0.08, 0.05–0.15, 0.05–0.25 and 0.05–0.40, respectively.

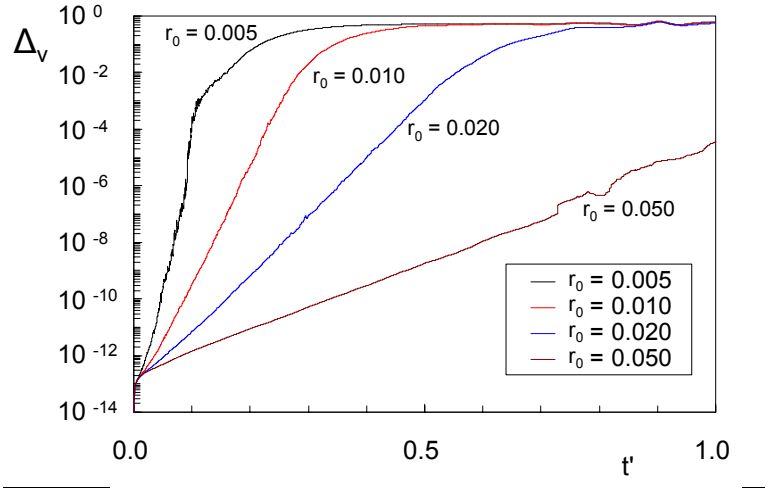

Fig. 5. (Color online) Time evolutions of the trajectory distance $\Delta_v(t')$ for various softening parameters r_0 with $t_{\rm rev} = 1.0$. The origin of t' is the time $t_{\rm rev}$ of the time-reversal operation.

increases with $t_{\rm rev}$. Moreover, as expected, Δ_{vf} increases with decreasing softening parameter r_0, since the extent of the instability of the system increases with decreasing r_0. That is, under the restriction of constant initial energy, both the instability and the propagation of numerical irreversibility due to round-off errors depend on the softening parameter r_0 in the same way.

In Paper I, to observe the behavior of numerical irreversibility universally, we proposed the use of a propagation time $\tau_{\rm p}$ based on the normalized ratio of velocity moments VM which was appropriate because we were considering the system at various energy states. However, in the present study, since the initial energy is approximately fixed, the time evolutions of VM are not very different from each other. That is, $\tau_{\rm p}$ is not suitable for the present case. Therefore, using the Lyapunov time t_λ, we re-plot the final trajectory distance Δ_{vf} against $t_{\rm rev}/t_\lambda$. Note that although t_λ described in Table 2 is calculated from the result for $t_{\rm rev} = 1.0$, we have confirmed that t_λ does not greatly depend on $t_{\rm rev}$ in the present study.

As shown in Fig. 7, for smaller values of the final trajectory distance ($\Delta_{vf} \lessapprox$

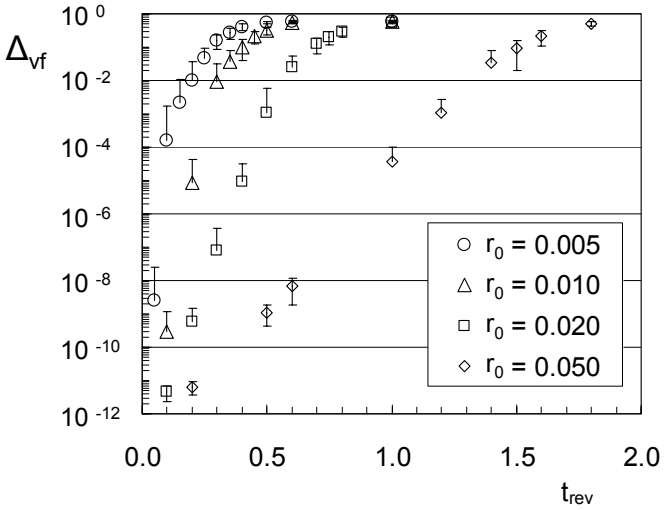

Fig. 6. Final trajectory distance Δ_{vf} for various softening parameters r_0. The error bars indicate the 68% confidence level in terms of the normal error distribution for approximately 100 simulations.

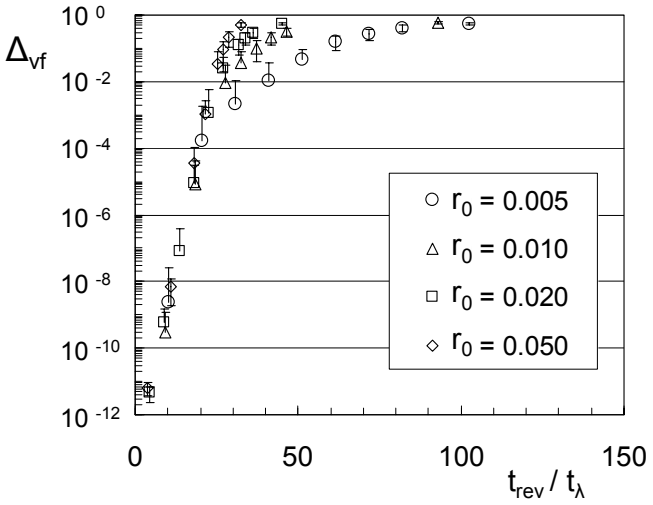

Fig. 7. Influence of the softening parameter on the final trajectory distance Δ_{vf}. The results shown in Fig. 6 are re-plotted against the time normalized by the Lyapunov time t_λ.

10^{-3}), the results for all the various softening parameters agree well with each other. Accordingly, for $\Delta_{vf} \lessapprox 10^{-3}$, the behavior of the numerical irreversibility is dominated by the Lyapunov time t_λ or the instability of the system. On the other hand, for $\Delta_{vf} \gtrapprox 10^{-3}$, the results are not on a common curve. This is because, as shown Fig. 6, for $\Delta_{vf} \gtrapprox 10^{-3}$, the final trajectory distance does not increase exponentially with the time $t_{\rm rev}$ of the time-reversal operation.

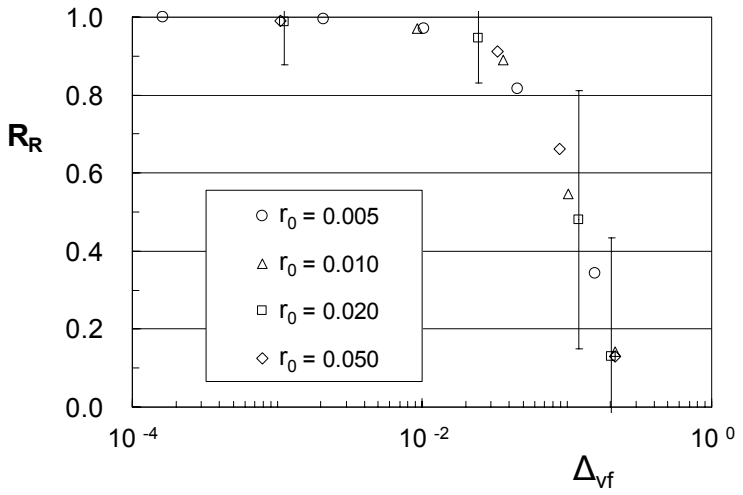

Fig. 8. Final trajectory distance Δ_{vf} and recovery rate R_R. For simplicity, the error bars for $r_0 = 0.020$ are taken to be typical.

In order to examine the characteristics of the numerical irreversibility appearing in the region $\Delta_{vf} \gtrapprox 10^{-3}$, we investigate the relationship between the final trajectory distance Δ_{vf} and the recovery rate R_R. As mentioned previously, the recovery rate measures the loss of reversibility in the present simulation; i.e., the smaller R_R, the more irreversible the system is. As shown in Fig. 8, R_R starts to decrease at $\Delta_{vf} \approx 10^{-3}$, although the numerical irreversibility due to round-off errors starts generating at the first time step of the time-reversible simulation. This is because the recovery rate measures the macroscopic behavior of the system, through the velocity distribution. After the final trajectory distance grows sufficiently large, we can observe the loss of reversibility or numerical irreversibility clearly. Moreover, we found that after $\Delta_{vf} \approx 10^{-3}$, all the results for various r_0 were on a common curve. This means that for $\Delta_{vf} \gtrapprox 10^{-3}$, the final trajectory distance Δ_{vf} and the loss of reversibility measured by R_R are closely related to each other.

By using the recovery rate R_R, we define a new quantity, the memory loss time $t_{\rm m}$, representing the time when the simulated trajectory completely forgets its initial conditions. That is, $t_{\rm m}$ represents the time required for $R_R = 0$. Figure 9 shows the influence of the softening parameter r_0 on $t_{\rm m}$ and the Lyapunov time t_λ. As shown in Fig. 9, not only t_λ but also $t_{\rm m}$ increases monotonically with r_0. In the present simulation, t_λ is shorter than the crossing time $\tau_c \approx 0.1$.

According to Kandrup et al. [21], the mean e-folding time for individual particle perturbations or the e-folding time for the total $3N$-dimensional configuration space perturbation can be fitted by a simple power law. We apply this idea to our simulation result, considering the Lyapunov time t_λ calculated

from the trajectory distance in velocity speed space. t_λ can be given as

$$t_\lambda(r_0) = A_1 \times (r_0)^{p_\lambda} + B_1, \tag{15}$$

where p_λ, A_1 and B_1 are constant values. The best-fit value obtained from Fig. 9 is $p_\lambda \approx 1.0$ and therefore we can expect that t_λ increases approximately linearly with the softening parameter r_0. Similarly, the memory loss time $t_{\rm m}$ could be given as

$$t_{\rm m}(r_0) = A_2 \times (r_0)^{p_{\rm m}} + B_2, \tag{16}$$

where $p_{\rm m}$, A_2 and B_2 are constant values. Since the best-fit value is $p_{\rm m} \approx 1.0$, $t_{\rm m}$ defined here also seems to increase approximately linearly with r_0. However, as shown in Fig. 9, $t_{\rm m}$ is longer than both the crossing time τ_c and t_λ. This is because, as mentioned previously, $t_{\rm m}$ is based on the recovery rate R_R, which measures the macroscopic behavior of the system through the velocity distribution.

In order to examine the memory loss time $t_{\rm m}$ more clearly, we re-plot $t_{\rm m}$ against the Lyapunov time t_λ. As shown in Fig. 10, $t_{\rm m}$ increases approximately linearly with t_λ in the present small self-gravitating system. However, we note that, as discussed in Paper I, if the instability affected by the softening parameter is fixed, the propagation of numerical irreversibility is dominated by early relaxation processes or energy states. Therefore, we can conclude that both the energy state of the system and the instability affected by the softening parameter influence the loss of reversibility or the propagation of numerical irreversibility appearing in the self-gravitating system.

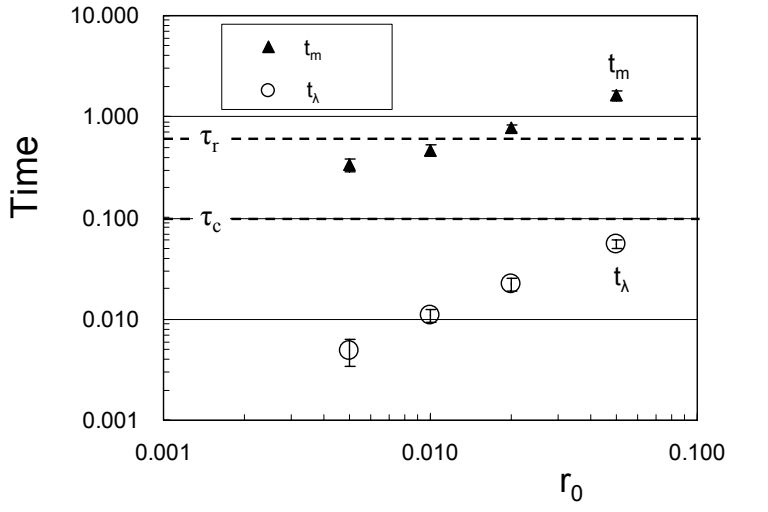

Fig. 9. Influence of the softening parameter r_0 on the memory loss time $t_{\rm m}$ and the Lyapunov time t_λ. The horizontal broken lines represent the crossing time $\tau_c \approx 0.1$ and the relaxation time $\tau_r \approx 0.6$. The error bars for $t_{\rm m}$ are evaluated from those for $t_{\rm rev}$–R_R plots.

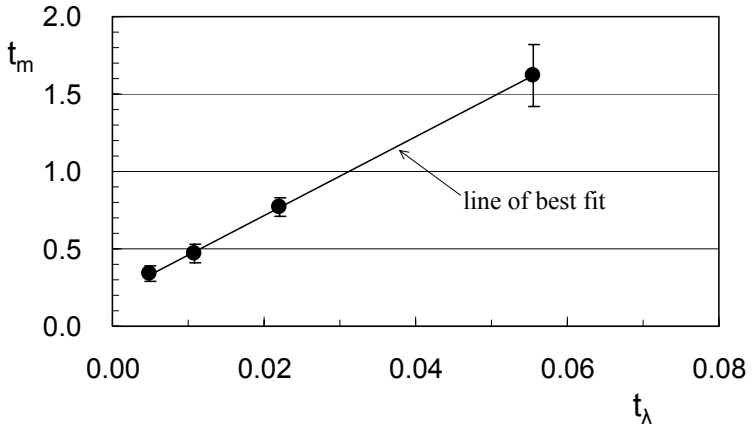

Fig. 10. Memory loss time $t_{\rm m}$ and Lyapunov time t_λ.

The N-dependence of the e-folding time t_e has been discussed in detail in previous studies [8,20,22,26]. For example, t_e is estimated to be $t_e \sim 1/\ln(\ln N)$ for $N \approx 10^2$ [22] and $t_e \sim 1/\ln N$ for $N \approx 10^5$ [26]. Accordingly, by using these results, we can predict the N-dependence of the memory loss time.

3.3 Influence of the integration step size

To study the influence of the integration step size (i.e., the time step), Δt is varied ranging from 10^{-4} to 10^{-6}, for $r_0 = 0.005$ and $t_{\rm rev}$=0.1. In this subsection, for simulating more unstable systems, the softening parameter r_0 is set to be 0.005. The other specifications are the same as those in Sections 3.1 and 3.2.

As shown in Fig. 11, we can confirm that global errors $|\Delta\varepsilon_{\rm max}/\varepsilon_0|$ in total energy increase with Δt, where ε_0 and $\Delta\varepsilon_{\rm max}$ represent the initial total energy and the difference between the maximum and minimum total energies, $\varepsilon_{\rm max} - \varepsilon_{\rm min}$, during the simulation, respectively. This simulation result is consistent with the result in Paper I. On the other hand, the final trajectory distance Δ_{vf} seems to increase with decreasing Δt, because strong collisions or close encounters could occur more frequently when Δt is small. However, since the values of Δ_{vf} fluctuate widely, the influence of the time step isn't clear. (Note that all the recovery rates R_R are approximately 1.0 and don't depend on the integration step size in the present simulation. This is because $t_{\rm rev}$=0.1 is too short for R_R to start decreasing, since R_R starts to decrease at $\Delta_{vf} \approx 10^{-3}$.)

In order to examine the influence of the integration step size in detail, we

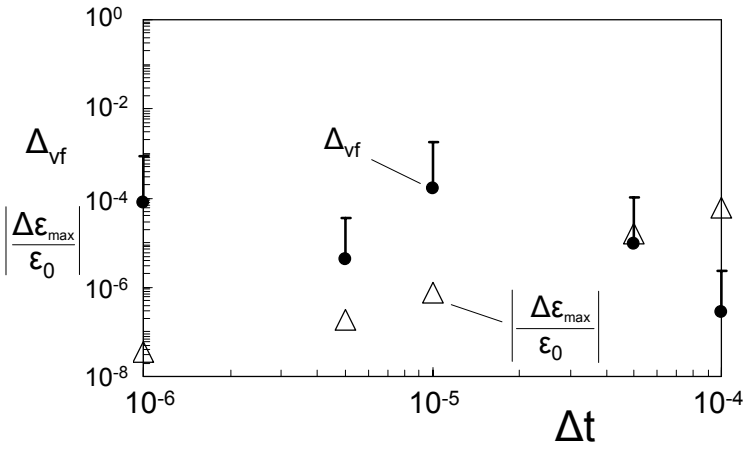

Fig. 11. Influence of the integration step size Δt, for $r_0 = 0.005$ and $t_{\rm rev}$=0.1. The closed circles and the open triangles represent the final trajectory distance Δ_{vf} and global errors $|\Delta\varepsilon_{\rm max}/\varepsilon_0|$ in total energy, respectively.

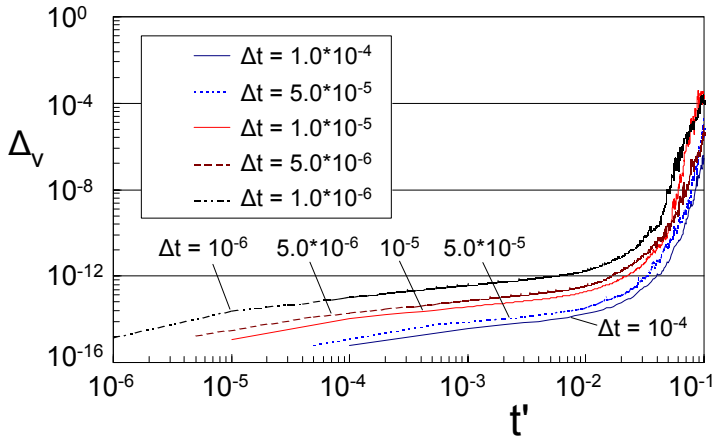

Fig. 12. (Color online) Time evolutions of the trajectory distance $\Delta_v(t')$ with various integration step sizes, for $r_0 = 0.005$ and $t_{\rm rev}$=0.1. The trajectory distance is plotted every $10\Delta t$ steps. The horizontal axis, t', is indicated by a logarithmic axis.

observe time evolutions of the trajectory distance $\Delta_v(t')$, where the origin of t' is the time $t_{\rm rev}$ of the time-reversal operation. As shown in Fig. 12, the initial values of the trajectory distance are the common one at the first time step, i.e., at $t' = 1\Delta t$. After the first time step, all the curves increase gradually with time and then they increase exponentially ($10^{-2} \lessapprox t'$). Although the curves fluctuate, the slope of the curves is approximately comparable to each other. The above fact is similar to the result in Paper I. However, the trajectory

distance doesn't grow sufficiently large at t' =0.1, since the time is short. In particular, for $10^{-2} \lessapprox t'$, $\Delta_v(t')$ fluctuates widely. Similarly, as shown in Fig. 11, the final trajectory distance Δ_{vf} fluctuates in the present simulation.

4 Conclusions

In the present paper, we investigated the fundamental characteristics of numerical irreversibility in self-gravitating small N-body systems, from the viewpoint of time-reversible dynamics. In this study, we considered a closed spherical system consisting of 250 point-particles, which interact through the Plummer softened potential. In order to investigate the influence of instability on numerical irreversibility, the softening parameter r_0 for the Plummer softened potential was varied from $0.005R$ to $0.050R$, under the restriction of constant initial energy or constant initial virial ratio $2E_{\mathrm{KE}_0}/|E_{\mathrm{PE}_0}|$.

To examine the influence of the softening parameter r_0, we first investigated the time evolutions of both the virial ratio $2E_{\mathrm{KE}}/|E_{\mathrm{PE}}|$ and the corrected virial ratio α $(=(2E_{\mathrm{KE}} - 4\pi R^3 P_{\mathrm{wall}})/|E_{\mathrm{PE}}|)$, without the time-reversal operation. We confirmed that the behaviors of these ratios were consistent with two time scales, the crossing time τ_c and the relaxation time τ_r. At the quasi-steady state, the deviation of α from 1 increased with increasing softening parameter. Then, through a time-reversible simulation based on a velocity inversion technique, we demonstrated that the numerical irreversibility due to round-off errors appeared more rapidly with decreasing softening parameter r_0. In other words, the higher the instability of the system, the earlier the memory of the initial conditions is lost. For smaller values of the final trajectory distance $(\Delta_{vf} \lessapprox 10^{-3})$, the final trajectory distance depends on the Lyapunov time t_λ in chaos theory. (Note that, in our simulation, Δ_{vf} seemed to increase with decreasing the integration step size Δt, for $r_0 = 0.005R$ and t_{rev}=0.1.) On the other hand, for $\Delta_{vf} \gtrapprox 10^{-3}$, i.e., after the final trajectory distance grows sufficiently large, numerical irreversibility measured by the recovery rate is clearly visible. In particular, for $\Delta_{vf} \gtrapprox 10^{-3}$, the recovery rate R_R is closely related to the final trajectory distance Δ_{vf}. We also found that the memory loss time t_{m}, which was defined by the recovery rate, increased approximately linearly with t_λ in the present small self-gravitating system.

It should be noted that, as discussed in Paper I, if the instability affected by the softening parameter is fixed, the propagation of the numerical irreversibility is dominated by early relaxation processes or energy states. Therefore, we concluded that both the energy state of the system and the instability affected by the softening parameter influence the loss of reversibility or the propagation of numerical irreversibility appearing in the self-gravitating system.

A Reflecting wall

In the present study, to simulate a self-gravitating N-body system enclosed in a spherical container with a reflecting wall, the set of equations of motion is integrated using Verlet's algorithm. Accordingly, a position of a particle at time $t + \Delta t$ is given by $\mathbf{x}(t + \Delta t) = 2\mathbf{x}(t) - \mathbf{x}(t - \Delta t) + \sum \mathbf{f}_j(t) \, (\Delta t)^2$, where $\mathbf{f}_j(t)$ is a partial force from the j-th particle on the particle, located at position $\mathbf{x}$ at time t. When the position $\mathbf{x}(t + \Delta t)$ of the particle is located outside of the spherical container or the reflecting wall, the position is reversed to mimic the reflecting wall. The method is summarized as follows.

Let us consider the motion of a single particle, as shown in Fig. A.1. In this figure, $\mathbf{x}_1$ and $\mathbf{x}_2$ represent the positions $\mathbf{x}(t)$ and $\mathbf{x}(t + \Delta t)$, respectively. In other words, the single particle moves from $\mathbf{x}_1$ to $\mathbf{x}_2$ (This is the trajectory before the reflection.). When the position $\mathbf{x}_2$ is located outside of the reflecting wall, the reflected position $\mathbf{x}_{2\mathrm{r}}$ is given as

$$\overrightarrow{\mathbf{ox}_{2\mathrm{r}}} = \overrightarrow{\mathbf{ox}_2} - 2\frac{(\overrightarrow{\mathbf{sx}_2} \cdot \overrightarrow{\mathbf{os}})}{|\overrightarrow{\mathbf{os}}|} \times \frac{\overrightarrow{\mathbf{os}}}{|\overrightarrow{\mathbf{os}}|}, \tag{A.1}$$

where $\mathbf{o}$ and $\mathbf{s}$ represent the center of the sphere and the point at the intersection of the reflecting wall with the trajectory, as shown in Fig. A.1. The notation $\overrightarrow{\mathbf{ab}}$ represents a vector from position $\mathbf{a}$ to $\mathbf{b}$. Since the reflected positions, e.g., $\mathbf{x}_{1\mathrm{r}}$, can be similarly calculated, the radial component of the velocity of the particle is reversed. The position $\mathbf{s}$ of the intersection is calculated, assuming that the line $\widehat{\mathbf{x}_1\mathbf{x}_2}$ is a straight line. Therefore, if the particle moves from $\mathbf{x}_{2\mathrm{r}}$ to $\mathbf{x}_{1\mathrm{r}}$, the reflected positions are $\mathbf{x}_2$ and $\mathbf{x}_1$, respectively; i.e., the

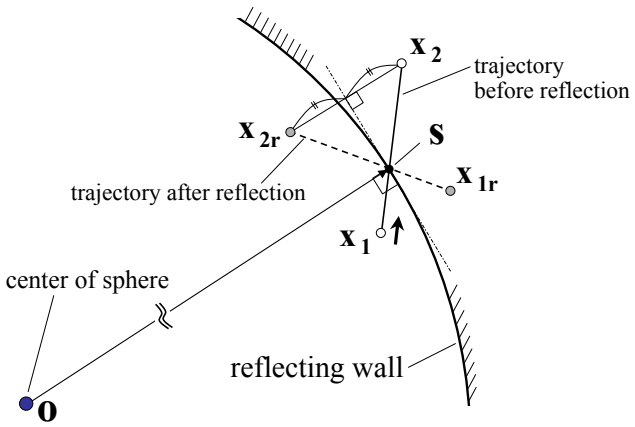

Fig. A.1. Reflecting wall and trajectory of the single particle.

radial component of the velocity of the particle is reversed similarly. Through several simulations with and without the reflecting wall, we have confirmed that our main result, e.g., the relationship between numerical irreversibility and instability, does not greatly depend on the above operation.

References

[1] V.A. Antonov, *in Dynamics of Globular Clusters*, edited by J. Goodman and P. Hut, IAU Symposium No. 113, (Reidel, Dordrecht, 1985); Vestn. Lening. Gos. Univ. 7 (1962) 135.

[2] D. Lynden-Bell, R. Wood, Mon. Not. R. Astron. Soc. 138 (1968) 495.

[3] J. Binney, S. Tremaine, *Galactic Dynamics*, Princeton University Press, Princeton, 1987.

[4] T. Padmanabhan, Phys. Rep. 188 (1990) 285.

[5] D. Lynden-Bell, Physica A 263 (1999) 293.

[6] C. Tsallis, J. Stat. Phys. 52 (1988) 479.

[7] V. Latora, A. Rapisarda, C. Tsallis, Phys. Rev. E 64 (2001) 056134.

[8] S.J. Aarseth, *Gravitational N-Body Simulations: Tools and Algorithms*, Cambridge University press, Cambridge, 2003.

[9] D.C. Heggie, P. Hut, *The gravitational million-body problem*, Cambridge University press, Cambridge, 2003.

[10] S.J. Aarseth, Mon. Not. R. Astron. Soc. 126 (1963) 223.

[11] R.H. Miller, Astrophys. J. 140 (1964) 250.

[12] R.H. Miller, J. Comput. Phys. 2 (1967) 1.

[13] M. Lecar, Bull. Astron. 3 (1968) 91.

[14] E.M. Standish, Ph. D. thesis, Yale Univ., 1968.

[15] V.G. Gurzadyan, G.K. Savvidy, Astron. Astrophys. 160 (1986) 203.

[16] H.E. Kandrup, Phys. Lett. A 140 (1989) 97.

[17] H.E. Kandrup, Physica A 169 (1990) 73.

[18] S.J. Aarseth, M. Lecar, Ann. Rev. Astron. Astrophys. 13 (1975) 1.

[19] Y. Suto, PASJ. 43 (1991) L9.

[20] H.E. Kandrup, H. Smith, Astrophys. J. 374 (1991) 255.

[21] H.E. Kandrup, H. Smith, D.E. Willmes, Astrophys. J. 399 (1992) 627.

[22] J. Goodman, D.C. Heggie, P. Hut, Astrophys. J. 415 (1993) 715.

[23] A.A. El-Zant, Astro. Astrophys. 326 (1997) 113.

[24] A.A. El-Zant, Astro. Astrophys. 331 (1998) 782.

[25] M. Cerruti-Sola, M. Pettini, Phys. Rev. E 51 (1995) 53.

[26] M. Hemsendorf, D. Merritt, Astrophys. J. 580 (2002) 606.

[27] D. Huber, D. Pfenniger, Astron. Astrophys. 386 (2002) 359.

[28] H.L. Wright, B.N. Miller, W.E. Stein, Astrophys. Space Sci. 84 (1982) 421.

[29] H.L. Wright, B.N. Miller, Phys. Rev. A 29 (1984) 1411.

[30] H.A. Posch, W.G. Hoover, Phys. Rev. A 38 (1988) 473.

[31] W.G. Hoover, *Time reversibility, Computer simulation, and Chaos*, World Scientific Publishing Co., 1999.

[32] Ch. Dellago, H.A. Posch, W.G. Hoover, Phys. Rev. E 53 (1996) 1485.

[33] J. Orban, A. Bellemans, Phys. Lett. 24A (1967) 620.

[34] Ch. Dellago, W.G. Hoover, Phys. Rev. E 62 (2000) 6275.

[35] G.E. Norman, V.V. Stegailov, Comput. Phys. Comm. 147 (2002) 678.

[36] N. Komatsu, T. Abe, Physica D 195 (2004) 391.

[37] N. Komatsu, T. Abe, Comput. Phys. Commun. 171 (2005) 187.

[38] N. Komatsu, T. Abe, Phys. Fluids 19 (2007) 056103.

[39] N. Komatsu, T. Kiwata, S. Kimura, Physica A 387 (2008) 2267.

[40] N.S. Krylov, *Works on the Foundations of Statistical Physics*, Princeton University Press, 1979.

[41] L. Hernquist, J.E. Barnes, Astrophysical Journal 349 (1990) 562.

[42] R.A. Gerber, Astrophysical Journal 466 (1996) 724.

[43] A.B. Romeo, Astronomy and Astrophysics 324 (1997) 523.

[44] H.E. Kandrup, I.V. Sideris, Phys. Rev. E 64 (2001) 056209.

[45] A.A. El-Zant, Mon. Not. R. Astron. Soc. 331 (2002) 23.

[46] D.J. Price, J.J. Monaghan, Mon. Not. R. Astron. Soc. 374 (2007) 1347.

[47] D. Merritt, Astronomical Journal 111 (1996) 2462.

[48] A.B. Romeo, Astronomy and Astrophysics 335 (1998) 922.

[49] E. Athanassoula, E. Fady, J.C. Lambert, A. Bosma, Mon. Not. R. Astron. Soc. 314 (2000) 475.

[50] W. Dehnen, Mon. Not. R. Astron. Soc. 324 (2001) 273.

[51] S. A. Rodionov, N. Ya. Sotnikova, Astronomy Reports 49 (2005) 470.

[52] H. Endoh, T. Fukushige, J. Makino, Publ. Astron. Soc. Japan 49 (1997) 345.

[53] A.A. El-Zant, Phys. Rev. E 58 (1998) 4152.

[54] I. Ispolatov, M. Karttunen, Phys. Rev. E. 68 (2003) 036117.

[55] I. Ispolatov, M. Karttunen, Phys. Rev. E. 70 (2004) 026102.

[56] A. Taruya, M. Sakagami, Physica A 307 (2002) 185.

[57] A. Taruya, M. Sakagami, Mon. Not. R. Astron. Soc. 364 (2005) 990.

[58] The unit of time in the present paper is the same as that for the figures and parameters (e.g., the integration step size, the crossing time, etc.) shown in Paper I.

[59] In several cases, the results are averaged over approximately 100 simulations, at least more than 95 simulations.

[60] If ε of the uniform state becomes lower than ε_{coll}, the system should undergo a collapse to a core-halo state. The collapse energy ε_{coll} is not greatly influenced by r_0: for example, for $r_0/R = 0$ and 0.005, the collapse energy is $\varepsilon_{coll} = -0.335$ and -0.339 [54], respectively.

[61] G.M. Zaslavsky, *Chaos in dynamic systems*, translated by V.I. Kisin, Harwood Academic Publishers, 1985.